Cellular prion protein targets amyloid-β fibril ends via its C-terminal domain to prevent elongation

Received for publication, April 5, 2017, and in revised form, August 15, 2017 Published, Papers in Press, August 23, 2017, DOI 10.1074/jbc.M117.789990

Erin Bove-Fenderson[‡], **Ryo Urano**[§], **John E. Straub**[§], **and David A. Harris**[‡1]

From the [‡]*Department of Biochemistry, Boston University School of Medicine, Boston, Massachusetts 02118 and the* [§]*Department of Chemistry, Boston University, Boston, Massachusetts 02215*

Edited by Paul E. Fraser

Oligomeric forms of the amyloid-β (Aβ) peptide are thought to represent the primary synaptotoxic species underlying the neurodegenerative changes seen in Alzheimer's disease. It has been proposed that the cellular prion protein (PrP^C) functions as a cell-surface receptor, which binds to Aβ oligomers and transduces their toxic effects. However, the molecular details of the PrP^C–Aβ interaction remain uncertain. Here, we investigated the effect of PrP^C on polymerization of Aβ under rigorously controlled conditions in which Aβ converts from a monomeric to a fibrillar state via a series of kinetically defined steps. We demonstrated that PrP^C specifically inhibited elongation of Aβ fibrils, most likely by binding to the ends of growing fibrils. Surprisingly, this inhibitory effect required the globular C-terminal domain of PrP^C, which has not been previously implicated in interactions with Aβ. Our results suggest that PrP^C recognizes structural features common to both Aβ oligomers and fibril ends and that this interaction could contribute to the neurotoxic effect of Aβ aggregates. Additionally, our results identify the C terminus of PrP^C as a new and potentially more druggable molecular target for treating Alzheimer's disease.

Alzheimer's disease (AD)[2] is associated with deposition in the brain of the amyloid-β (Aβ) peptide, a 40–42–amino acid cleavage product of the amyloid precursor protein (1). There is strong evidence that small oligomers of Aβ, rather than large, amyloid fibrils, represent the key neurotoxic species in AD (2). Aβ oligomers are thought to target synapses, causing both functional and structural changes at these sites (3, 4). Although the central importance of Aβ in AD is widely agreed upon, the mechanism by which it causes neuronal dysfunction has remained mysterious. It is presumed that the disease process starts by the binding of Aβ oligomers to receptor proteins or lipids on the surface of neurons. However, the molecular identity of the relevant binding sites is uncertain.

In 2009, Laurén *et al.* (5) identified the cellular prion protein (PrP^C) as a cell-surface receptor for soluble oligomers of the Aβ peptide, an observation subsequently confirmed by other groups (6–8). Binding of Aβ oligomers to PrP^C was shown to produce neurotoxic effects, including suppression of long-term potentiation and retraction of dendritic spines; it was reported that these effects depended upon interactions between PrP^C and metabotropic glutamate 5 receptor, resulting in activation of intracellular Fyn kinase (9–12). In addition, disruption of the endogenous gene encoding PrP^C was shown to rescue behavioral deficits as well as early mortality in certain AD transgenic models (13). Taken together, these results led to the proposal that PrP^C is one of the receptors mediating the synaptotoxic effects of Aβ oligomers and that pharmacologic targeting of PrP^C could represent a novel therapeutic strategy for treatment of AD (14–16). Although some studies have disputed the importance of PrP^C in mediating Aβ toxicity (17–20), these discrepancies may result from the use of different experimental paradigms, variability in preparations of synthetic Aβ oligomers, or the involvement of additional neurotoxic pathways.

Most previous studies of PrP^C–Aβ interaction have focused on oligomeric preparations of Aβ referred to as amyloid-β–derived diffusible ligands (ADDLs), which are produced by resolubilization of synthetic Aβ peptide in aqueous medium (21). ADDL preparations have the virtue of being enriched in soluble, oligomeric species, but they are very heterogeneous in terms of size, and they do not obviously correspond to any of the intermediate states that have been described during the polymerization of Aβ from a monomeric state. Under suitably controlled conditions, Aβ polymerizes by a well-studied process involving distinct steps of primary nucleation, secondary nucleation, and elongation (22–24). These kinetic steps have been mathematically modeled, and their rate constants have been determined (25–27). To explore more fully the nature of the PrP^C–Aβ interaction, we sought to determine how PrP^C affected the Aβ polymerization process and to use the results of these experiments to provide further insight into the nature of the Aβ species targeted by PrP^C. Our results have important implications for understanding the role of PrP^C as a receptor transducing the neurotoxic effects of Aβ, and they suggest a

This work was supported by National Institutes of Health (NIH) Grant R01 NS065244 (to D. A. H.), National Science Foundation Grant CHE-1362524 and NIH Grant R01 GM107703 (to J. E. S.), and National Research Service Award Fellowship 5F31NS090747 (to E. B-F.). The authors declare that they have no conflicts of interest with the contents of this article. The content is solely the responsibility of the authors and does not necessarily represent the official views of the National Institutes of Health.

This article contains supplemental Tables S1 and S2 and Figs. 1 and 2.

[1] To whom correspondence should be addressed: Dept. of Biochemistry, Boston University School of Medicine, K225, 72 E. Concord St., Boston, MA 02118. Tel.: 617-638-4362; Fax: 617-638-5339; E-mail: daharris@bu.edu.

[2] The abbreviations used are: AD, Alzheimer's disease; PrP^c, cellular prion protein; Aβ, amyloid-β; ADDLs, amyloid-β-derived diffusible ligands; ThT, thioflavin T; SEC, size-exclusion chromatography; HFIP, 1,1,1,3,3,3-hexafluoro-2-propanol; SDD-AGE, semidenaturing detergent agarose gel electrophoresis; FP, fluorescence polarization; SPR, surface plasmon resonance; DELFIA, dissociation-induced lanthanide fluorescence immunoassay; RU, resonance units; TCEP, tris(2-carboxyethyl)phosphine; TEV, tobacco etch virus.

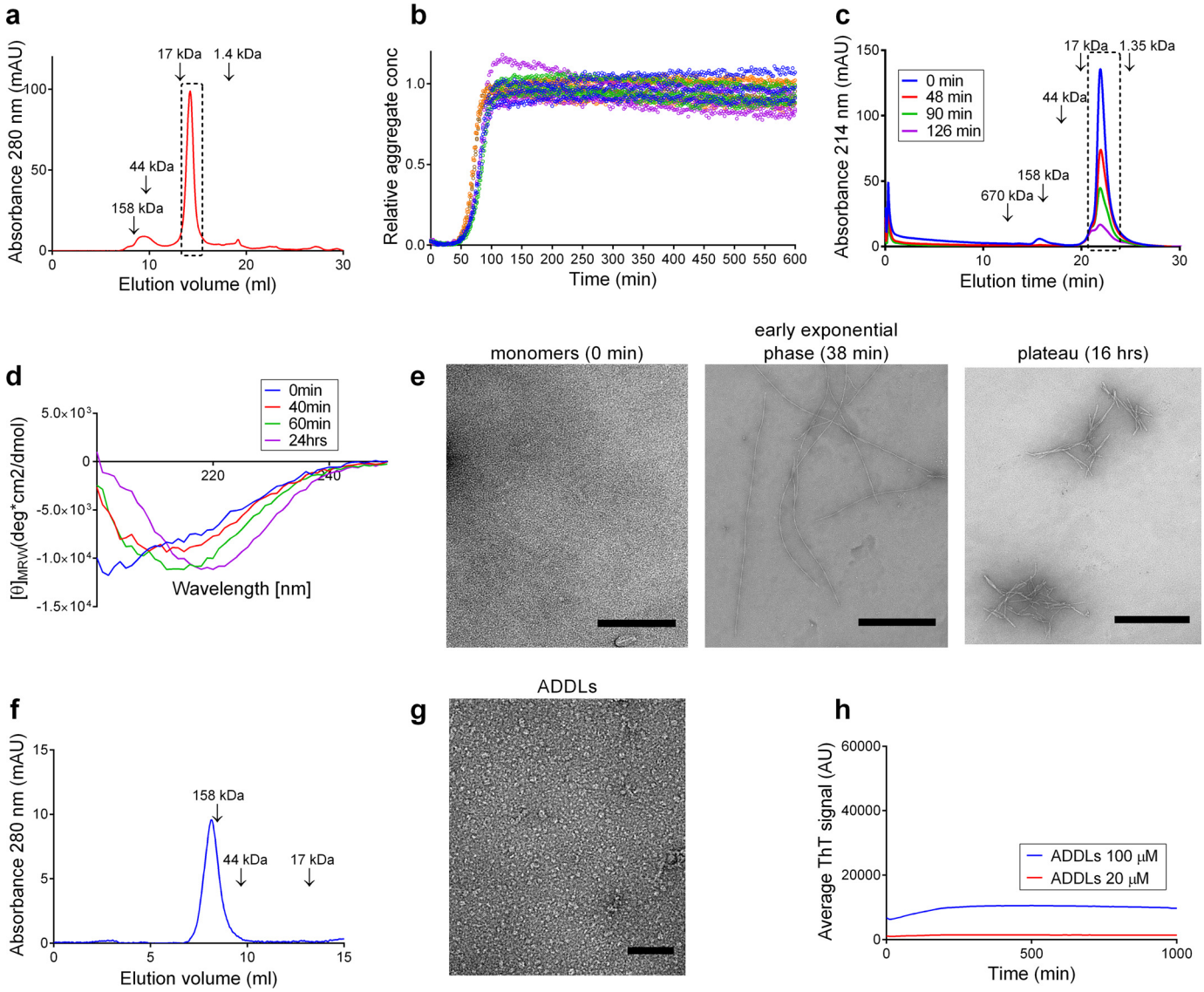

Figure 1. Preparation and polymerization of Aβ. *a*, size-exclusion chromatograph for preparation of Aβ monomers on a Superdex 75 column. *Rectangle*, the Aβ monomer peak collected for use in kinetic experiments. *Arrows*, elution volume of molecular weight standards. *b*, polymerization of Aβ (5 μM) monitored with ThT. Each set of *colored* dots represents one polymerization run with triplicate samples (for a total of seven polymerization runs). *c*, analytical SEC (Agilent Bio Sec-3 column) of samples taken at different times from the polymerization reaction shown in *b*. *Arrows*, molecular weight standards. Samples were centrifuged and filtered to remove insoluble aggregates before injection into the column. *d*, far-UV circular dichroism of Aβ at the indicated times during the course of polymerization. The CD signature shifts from random coil to β-sheet. *e*, EM images of negatively stained preparations of Aβ (10 μM) taken at 0 min (monomers), 38 min (early exponential phase), and 16 h (plateau phase). *Scale bars*, for monomer, 200 nm; for 38 min and 16 h, 500 nm. Samples were concentrated by centrifugation before imaging. *f*, SEC of ADDLs on a Superdex 75 column, showing a peak in the void volume. *g*, EM of negatively stained ADDLs showing small globular aggregates. *Scale bar*, 500 nm. *h*, ThT curves for ADDLs incubated under the same conditions used for polymerization of Aβ monomers shown in *b*. The ThT signal is much lower than in *b* and does not change substantially over 16 h.

novel approach for disrupting the PrP^C–Aβ interaction for therapeutic purposes.

Results

Aβ preparation and polymerization

We used carefully defined conditions for polymerization of Aβ(1–42) (hereafter referred to simply as Aβ), which have been described previously (22, 23, 28, 29) and which have been shown to result in reproducible kinetic curves as monitored by thioflavin T (ThT) fluorescence. To ensure that our experiments began with monomeric Aβ, we solubilized lyophilized peptide in 15 mM NaOH and used a Superdex 75 column to isolate monomers (Fig. 1*a*). Aβ in the monomer fraction produced a random coil signature by circular dichroism (Fig. 1*d*, *0 min curve*), consistent with the absence of significant β-sheet–containing aggregates.

Upon incubation in physiological buffer, monomeric Aβ polymerized in a highly reproducible fashion based on ThT fluorescence, following characteristic sigmoidal kinetics (Fig. 1*b*). Starting with a monomeric Aβ concentration of 5 μM, polymerization proceeded with a typical lag time of 50–60 min, reaching a plateau after about 90–100 min, with a half-time of 70–80 min. Using analytical size-exclusion chromatography (SEC), we observed continuous depletion of monomers in the Aβ sample over time, reflecting their incorporation into filaments that were removed by filtration and ultracentrifugation

before chromatography (Fig. 1*c*). We did not detect a significant population of oligomeric species that migrated with a molecular size of ≤100 kDa at any time during the course of polymerization. This observation is consistent with previous reports that oligomers, although obligate intermediates during the polymerization process, never constitute >1% of the total Aβ mass during the course of the reaction, with the major species being monomers and fibrils, the ratio of which changes continuously as polymerization proceeds (22). During the polymerization process, the CD signature of the Aβ gradually shifted from random coil to β-sheet, consistent with incorporation of unstructured monomers into amyloid fibrils (Fig. 1*d*).

Using electron microscopy with negative staining, we observed that fibrils formed early during the polymerization process, consistent with previous reports that fibrils are first detectable during the lag phase (30, 31) (Fig. 1*e*, *center image*). During the early exponential phase, the fibrils had lengths of 0.5–2 μm and displayed a twisted morphology with diameters ranging between 4.1 ± 0.8 nm in the narrow regions and 12.1 ± 1.5 nm in the thick regions. At later time points, fibrils tended to clump together, and their lengths and morphology were more difficult to discern (Fig. 1*e*, *right image*). These structural features have been described previously (32). Only scattered fibrils were observed in the isolated monomer fraction at zero time, and these were much more difficult to locate on the EM grid. For the most part, fibrils were not detected on the surface of the grid when freshly prepared Aβ was applied (Fig. 1*e*, *left image*). Most likely, the scattered fibrils that were observed represent a very small proportion of the total Aβ present at this time point and are a reflection of how rapidly aggregates begin to form after monomers of Aβ are isolated.

For the purposes of comparison, we utilized ADDL preparations in some of the experiments described below. ADDLs are typically prepared by solubilizing Aβ in HFIP, drying to a thin film, resuspending the film in DMSO, diluting into aqueous medium, and incubating for 16 h at room temperature. These preparations consisted primarily of aggregates that eluted in the void volume of the Superdex 75 column, indicating a molecular size > 70 kDa (Fig. 1*f*). As described previously (21), these aggregates appeared as small, globular assemblies of 5–10 nm in diameter by EM (Fig. 1*g*). The ThT-binding signal obtained from ADDL preparations, even at 20 or 100 μM, was considerably lower than the maximum signal achieved by fully polymerized Aβ at 5–10 μM, consistent with the absence of long fibrils in the ADDL samples (Fig. 1*h*). The ThT signal of the ADDL preparations did not increase further with continued incubation, indicating that the aggregates did not fibrillize during the 16-h period after formation.

PrP delays fibril formation at substoichiometric ratios

We sought to determine what effect PrP has on the polymerization process itself. We found that recombinant PrP profoundly delays Aβ polymerization, even when present in amounts that are highly substoichiometric to Aβ (Fig. 2*a*). The half-time for polymerization was nearly doubled at a PrP/Aβ ratio of 1:160 and tripled at a ratio of 1:20 (Fig. 2*b*). However, even in the presence of PrP, polymerization eventually reached the same plateau value of ThT binding, indicating that PrP at the concentrations examined slowed, but did not prevent, conversion of monomeric to fibrillar Aβ.

The inhibitory effect of PrP on Aβ fibril formation could also be visualized using semidenaturing detergent agarose gel electrophoresis (SDD-AGE), which provides a means of separating large, SDS-resistant amyloid fibrils from monomers and smaller aggregates on agarose gels. After 160 min, samples polymerized without PrP, which had reached the plateau phase of ThT binding, contained substantial amounts of fibrillar material, which migrated as a broad smear (Fig. 2*c*, *lane 6*). At this same time point, samples polymerized in the presence of increasing amounts of PrP contained decreasing amounts of fibrillar material on SDD-AGE (Fig. 2*c*, *lanes 1–5*), corresponding to the lower levels ThT binding reached by these samples. When SDD-AGE analysis was performed at 16 h, when plateau values of ThT fluorescence had been attained in all samples, there was no apparent difference in the amount of fibrillar material between PrP-containing and control reactions (Fig. 2*d*), again indicating that PrP in substoichiometric amounts slows but does not completely prevent fibril formation.

We also assessed the effect of PrP on polymerization of fluorescently labeled Aβ using fluorescence polarization (FP). In both the presence and absence of PrP, polarization increased with time, reflecting incorporation of labeled Aβ monomers into fibrils, which have a lower rotational mobility (Fig. 2*e*). This change in polarization was slower in the presence of PrP, consistent with an inhibitory effect on fibril formation. The FP signal plateaued at a similar value with and without PrP, suggesting again that PrP delayed but did not prevent fibril formation, with all of the monomers eventually being converted to the fibrillar form.

PrP does not prevent secondary nucleation by preformed fibrils

When a small amount of preformed fibrils is added at the start of an Aβ aggregation reaction, the rate-limiting, primary nucleation step is bypassed, shortening the lag phase and resulting in rapid formation of new fibrils by secondary nucleation and elongation (22). We investigated how PrP affected this process. We seeded a solution of 5 μM Aβ with a 1% molar equivalent of preformed fibrils in the presence and absence of PrP and compared the results with equivalent unseeded reactions. As expected, in the absence of PrP, seeding significantly accelerated the polymerization reaction (Fig. 3*a*, *0 nM curve*). PrP showed an inhibitory effect in seeded reactions (Fig. 3*a*), gradually damping the acceleration produced by the seeds. Importantly, however, the strength of the effect was reduced when compared with non-seeded reactions with equivalent amounts of PrP (Fig. 3*b*). For each concentration of PrP, the half-time was significantly decreased by the addition of seeds (Fig. 3*c*). This result held true independent of whether PrP was preincubated with the fibrils before their addition to the reaction (not shown). In another variation of the experiment, we found that fibrils formed in the presence of PrP accelerated polymerization reactions to nearly the same extent as fibrils formed in the absence of PrP (Fig. 3, *d* and *e*). Taken together, these results suggest that PrP does not have a major effect on the secondary

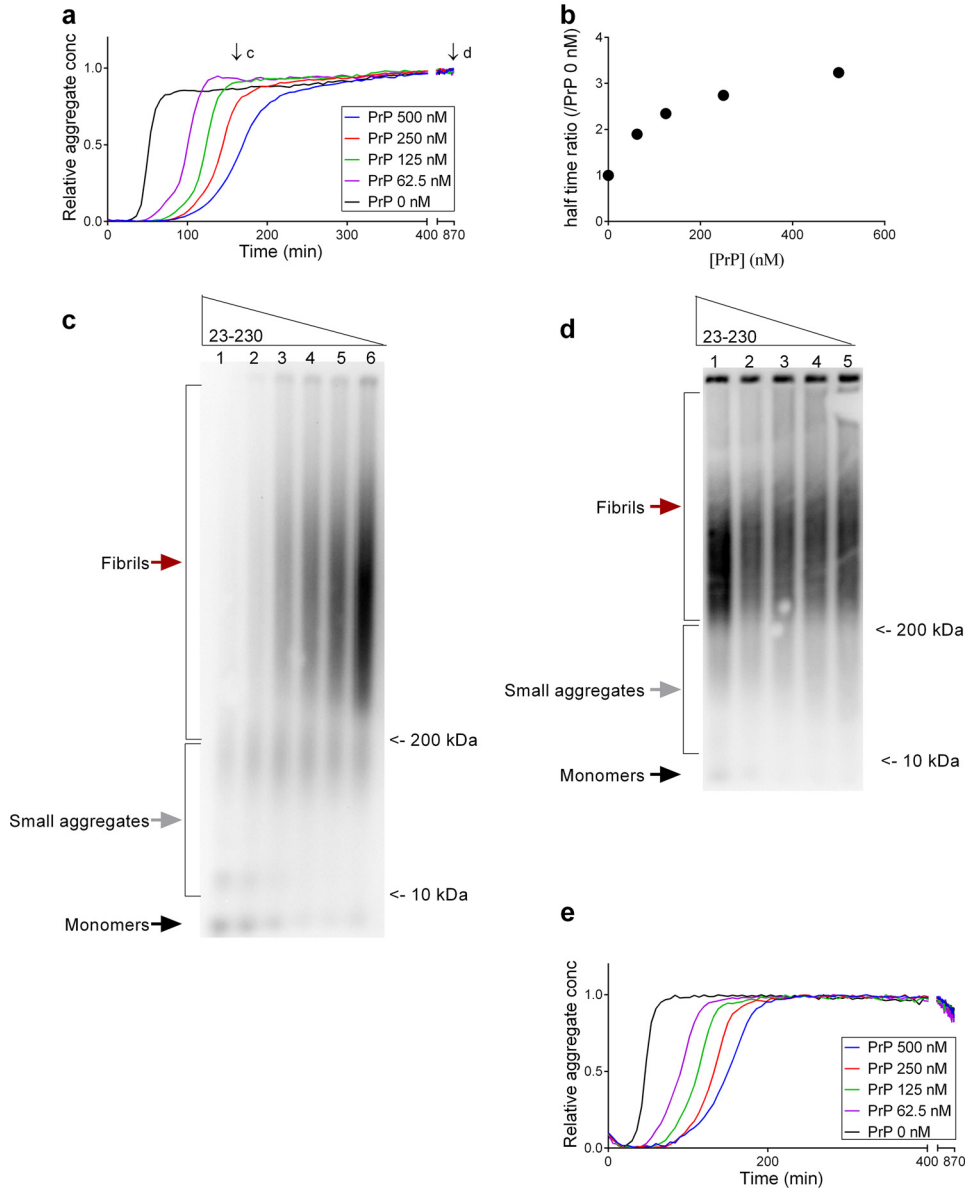

Figure 2. PrP inhibits Aβ polymerization at substoichiometric ratios. *a*, ThT curves for polymerization of Aβ (10 μM) in the presence of increasing concentrations of PrP. *Arrows*, approximate time points at which samples were removed for the SDD-AGE analyses shown in *c* and *d* (samples for *c* were taken from a separate experiment that included an additional concentration of PrP, not shown). *b*, effect of PrP on the half-times for Aβ polymerization, derived from the data in *a*. *Symbols* represent the means of three replicates. Error bars are not visible due to the small variance of the data (±1–2 min). *c* and *d*, SDD-AGE analysis of Aβ samples in the presence of different amounts of PrP. Samples were polymerized for 160 min (*c*) or 16 h (*d*). PrP concentrations for *c* were 500 nM (*lane 1*), 250 nM (*lane 2*), 125 nM (*lane 3*), 62.5 nM (*lane 4*), 31.2 nm (*lane 5*), and 0 nM (*lane 6*). PrP concentrations for d were 500 nM (*lane 1*), 250 nM (*lane 2*), 125 nM (*lane 3*), 62.5 nM (*lane 4*), and 0 nM (*lane 5*). Blots of the gels were probed with anti-Aβ antibody 6E10. The migration of 10 and 200 kDa molecular size markers is indicated, as are the positions of monomers, small aggregates, and fibrils. *e*, FP curves for polymerization of Hilyte-488 Aβ (10 μM) in the presence of increasing concentrations of PrP.

nucleation phenomena that occur when reactions are seeded by preformed fibrils.

PrP selectively inhibits filament elongation

Given the mechanistically well-characterized features of Aβ polymerization under the controlled experimental conditions we employed, we had an opportunity to pinpoint which microscopic step(s) were being affected by PrP using a mathematical modeling approach based on the macroscopic ThT curves. This approach has been used successfully to characterize interactions between Aβ and several molecular chaperones (23). We first determined the integrated rate law for Aβ aggregation in the absence of PrP, using as a guideline published values for the key rate constants (see supplemental material). We then fit the ThT curves in the presence of PrP by systematically varying the rate constant for only one of the three molecular steps in the polymerization process: k_n for primary nucleation, k_2 for secondary nucleation, and k_+ for elongation. The best global fit to the data was achieved when the elongation rate (k_+) was varied in response to PrP addition (Fig. 4*a*). The sum of residual errors for this fit was 1.7, compared with 7.7 and 17.7 for the fits to variations in k_n and k_2, respectively (Fig. 4, *b* and *c*). The calculated values for k_+ exhibit a strong influence of PrP concentration on elongation rate, which dropped to 6% of the uninhibited value in the presence of 250 nM PrP, a 1:12 ratio of PrP to Aβ (Fig. 4*a* (*inset*), and supplemental Tables S1 and S2).

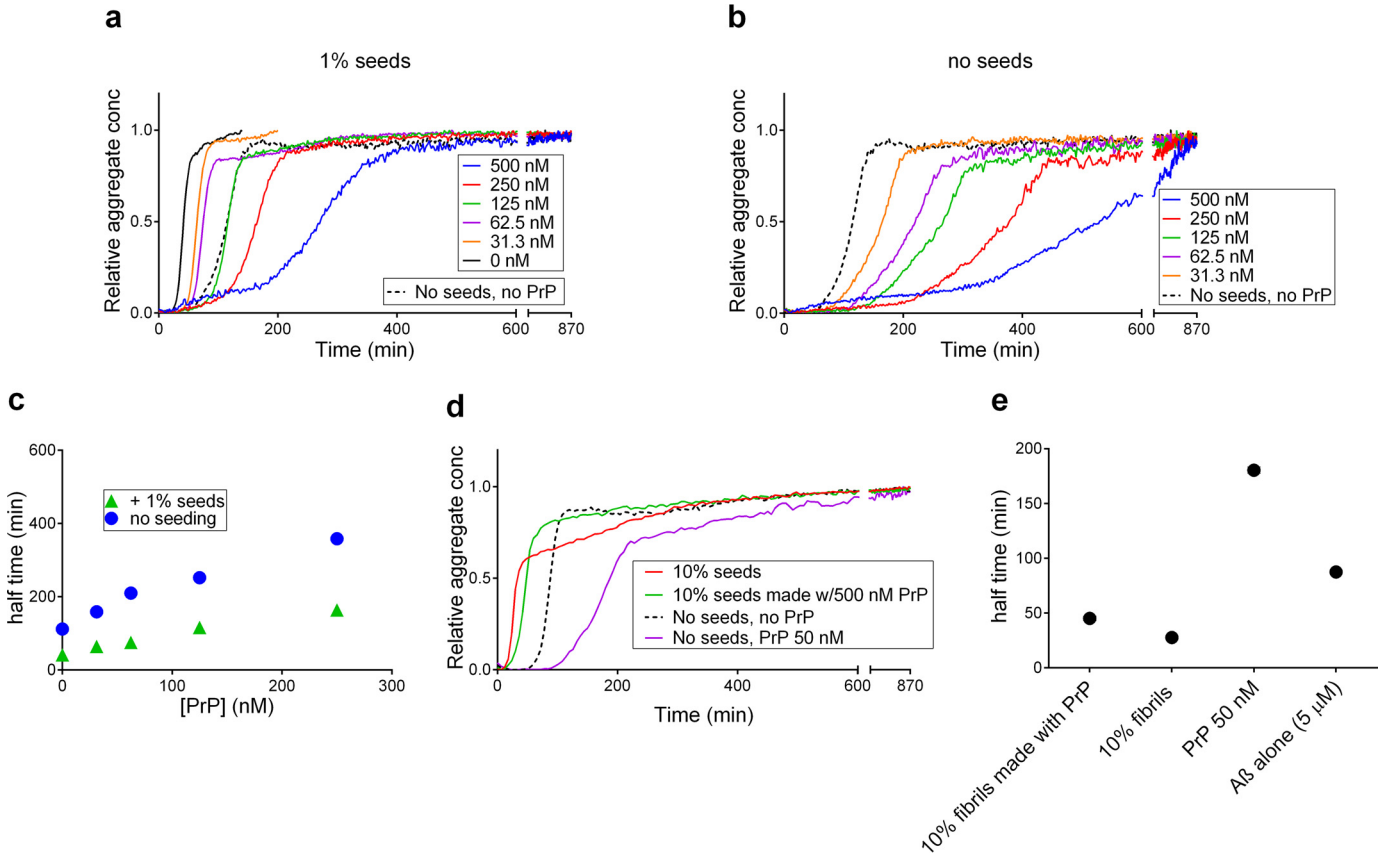

Figure 3. PrP does not prevent secondary nucleation by preformed fibrils. *a*, ThT curves for the seeded polymerization of Aβ (5 μM) in the presence of PrP. Seeding was achieved by the addition of 1% monomer equivalent of preformed Aβ fibrils to the reaction at zero time. The *black*, *dashed line* shows unseeded polymerization without PrP. *b*, ThT curves for the unseeded polymerization of Aβ (5 μM) in the presence of increasing concentrations of PrP. *c*, effect PrP on the half-times for Aβ polymerization in the seeded and unseeded conditions, derived from the data in *a* and *b*. *Symbols* represent the means of three replicates. *Error bars* are not visible due to the small variance of the data (±1–2 min). *d*, polymerization of Aβ (5 μM) was seeded by the addition of 10% monomer equivalent of fibrils formed in the presence (*green line*) or absence (*red line*) of 500 nM PrP. Unseeded control reactions contained no PrP (*dotted black line*) or 50 nM PrP (*purple line*), which is the amount that would be carried over by the addition of 10% seeds formed with 500 nM PrP. *e*, half-times of polymerization were calculated from the *curves* in *d*. *Symbols* represent the means of three replicates. Error bars are not visible due to the small variance of the data (±1–2 min).

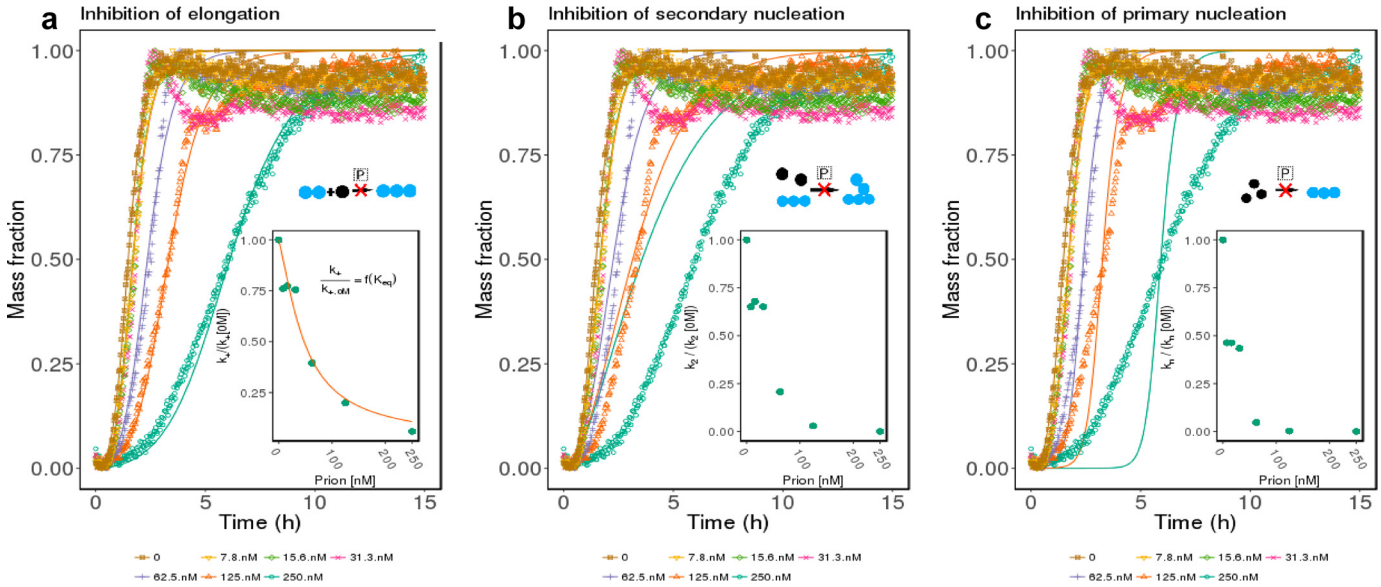

Figure 4. PrP selectively inhibits filament elongation. The *dotted symbols* show ThT polymerization curves for 3 μM Aβ in the presence of the indicated concentrations of PrP. The *solid lines* show best global fits to the data based on varying the kinetic constants for elongation rate, k_+ (*a*), secondary nucleation rate, k_2 (*b*), or primary nucleation rate, k_n (*c*). The *schematics* in each *panel* illustrate the step in the polymerization process at which PrP (denoted by *P*) is assumed to act. The *insets* show the variation in the respective rate constants as a function of PrP concentration, normalized to the value in the absence of PrP. The *solid line* in the *inset* of *a* is fit to the data points based on PrP binding to fibril ends with $K_{eq} = 2.1 \times 10^7\ M^{-1}$. See the supplemental materials for details.

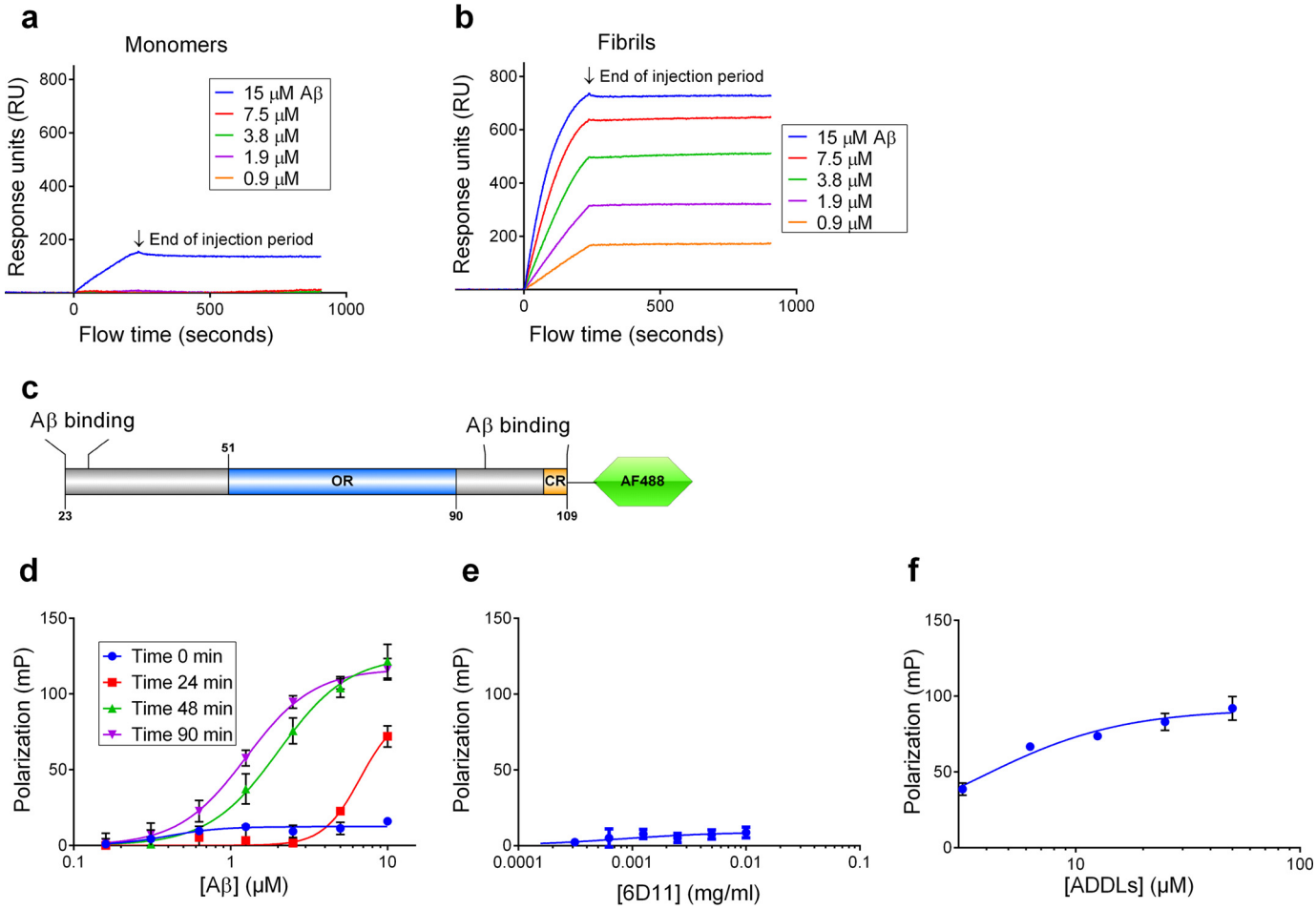

Figure 5. PrP binds to Aβ monomers, fibrils, and ADDLs with different affinities. *a*, monomeric Aβ at the indicated concentrations was injected over a chip containing immobilized PrP for 240 s, followed by a wash with buffer alone. Sensorgrams show binding in RU. *b*, fibrillar Aβ that had been polymerized for 16 h was subjected to SPR analysis as in *a*. *c*, diagram for Alexa Fluor 488–labeled PrP(23–109) used as a probe in fluorescence polarization experiments. *d*, fluorescence polarization of Alexa Fluor 488–labeled PrP(23–109) (25 nM) bound to Aβ (10 μM) sampled at the indicated times after initiation of polymerization: monomer (0 min); mid-lag phase (24 min); exponential phase (48 min); plateau (90 min). *e*, FP for binding of anti-PrP antibody 6D11 to Alexa Fluor 488–labeled PrP(23–109). *f*, FP for binding of ADDLs to Alexa Fluor 488–labeled PrP(23–109).

As Aβ fibrils are thought to grow by monomer addition to the fibril ends (22), a plausible mechanism for the inhibitory effect of PrP on fibril elongation is that PrP binds specifically to the growing ends of the fibrils, preventing monomer addition. If one assumes that PrP is present in excess and that it binds rapidly to fibril ends as soon as they are generated (*i.e.* that binding is at equilibrium), it is possible to derive a mathematical expression, in the form of a Langmuir binding isotherm, relating the normalized values for k_+ to the concentration of PrP. This expression incorporates an equilibrium constant, K_{eq}, for binding of PrP to the fibril ends. The experimentally determined k_+ values in the presence of increasing concentrations of PrP provide an excellent fit to this model (Fig. 4*a*, *inset*), yielding a value for K_{eq} of 2.1×10^7 M^{-1}, corresponding to an affinity constant of 47.6 nM. This quantitative analysis provides strong evidence that PrP selectively inhibits elongation of Aβ fibrils and suggests that it does so by binding tightly and selectively to fibril ends.

PrP binds both monomeric and fibrillar forms of Aβ but with different affinities

To provide biochemical evidence for this model, we examined binding interactions between PrP and the two major species present during the polymerization reaction: monomers and fibrils. For comparison, we also analyzed PrP binding to ADDLs, an interaction that has been previously characterized. We employed three different techniques: surface plasmon resonance (SPR), dissociation-enhanced lanthanide fluorescence immunoassay (DELFIA), and FP.

For SPR experiments, we tagged recombinant PrP with a c-Myc epitope at its C terminus and captured it on the SPR chip using 9E10 antibody. This strategy was adopted to leave the N-terminal domain of PrP, which contains the two putative Aβ-binding sites, free to interact with Aβ that was injected over the chip in the mobile phase. We compared the binding ability of Aβ samples taken at 0 min, representing mainly monomer, and at 16 h, representing fully polymerized fibrils. We found that the 0-min sample displayed detectable binding (~180 resonance units (RU) after 240 s of injection) only at the highest concentration of Aβ (15 μM) (Fig. 5*a*). The 16-h sample gave much larger responses, ranging from 180 to 700 RU over a concentration span of 0.9–15 μM (Fig. 5*b*), presumably reflecting the larger molecular weight of fibrils compared with monomers. ADDLs also bound to PrP, consistent with previous reports, with response magnitudes intermediate between mono-

mers and fibrils (supplemental Fig. 1*a*). These results demonstrate that PrP binds efficiently to fully polymerized Aβ fibrils and to ADDLs. PrP may also bind weakly to Aβ monomers, although the much smaller mass of monomers compared with fibrils would make binding of this species more difficult to detect. It was not possible to calculate reliable affinity constants and stoichiometries for the PrP-Aβ binding reaction from these SPR data due to the fact that binding of the analyte (Aβ) did not reach saturation during the injection phase. These anomalies of PrP-Aβ interactions in SPR experiments have been noted before (6), and may be related to rebinding or self-association of Aβ.

To assess PrP-Aβ interactions under equilibrium conditions, we employed DELFIA. Aβ samples were incubated in plastic wells containing immobilized PrP, and the amount of bound Aβ was then measured using anti-Aβ antibody 6E10. We observed binding of monomers (0 min, both fresh and frozen), fibrils (16 h), and ADDLs, with apparent dissociation constants of 1.07 ± 0.34 μM for fibrils and 0.11 ± 0.04 μM for ADDLs (supplemental Fig. 1*b*). Monomer binding did not approach saturation; therefore, the dissociation constant was not calculated. The actual K_d values for the aggregated species are likely to be much lower than the apparent values, because the molar concentration of these forms is only a fraction of the total Aβ concentration by a factor equivalent to the number of subunits in each aggregate. Thus, this assay confirms that PrP binds Aβ monomers, polymers, and ADDLs, with a higher affinity for the latter two species.

If PrP binds selectively to the ends of Aβ fibrils, then the amount of binding should be directly related to the effective concentration of fibril ends in the Aβ sample. To test this prediction, we used DELFIA to compare binding of PrP to fibrils before and after shearing of the fibrils via sonication. A sample of sonicated fibrils should contain a larger number of fibril ends compared with an unsonicated sample at the same concentration. As predicted, sonication of fibrils increased PrP binding (supplemental Fig. 2).

Both SPR and DELFIA are surface-based binding techniques, which may be subject to artifacts resulting from potential interference by the substrate with the binding interaction between PrP and Aβ. We therefore tested PrP-Aβ interactions using FP, a solution-based technique. As the fluorescent probe, we utilized an N-terminal fragment of PrP (residues 23–109), which encompasses the two previously identified binding regions for Aβ aggregates (5, 6). This fragment was labeled on a C-terminal cysteine residue with Alexa Fluor 488 C_5 maleimide (Fig. 5*c*). We compared the change in polarization for samples taken at different time points of an Aβ polymerization reaction (Fig. 5*d*). The zero time (monomer) sample did not produce a polarization shift, whereas the samples taken at 24 min (lag phase), 48 min (early exponential phase), and 90 min (plateau phase) produced progressively greater shifts at equivalent Aβ concentrations. These results demonstrate that PrP(23–109) binds to Aβ fibrils that form during the polymerization process. The data do not necessarily indicate a lack of binding to monomers (M_r = 4,500), which would be too small to produce a measurable shift in FP values, as demonstrated by the fact that an even larger ligand, an anti-PrP antibody (M_r = 150,000), did not cause a shift in polarization (Fig. 5*e*). However, ADDLs did produce a polarization shift consistent with a size intermediate between monomers and fibrils (Fig. 5*f*).

The structured, C-terminal domain of PrP is required for inhibition of Aβ fibril elongation and also influences binding to monomers

It has been shown previously that the unstructured N-terminal domain of PrP contains two polybasic regions (residues 23–27 and 95–105), which are required for binding to ADDLs, whereas the globular C-terminal domain is dispensable for this function (Fig. 6*a*, *top schematic*) (5, 6). We tested the roles of the N- and C-terminal domains in the ability of PrP to inhibit the growth of Aβ fibrils. Fig. 6*a* shows schematic diagrams of the deletion constructs used for these experiments.

As expected, removing the entire N-terminal domain (yielding construct 110–230) completely abolished the inhibitory effect of PrP on Aβ fibrillation (Fig. 6, compare *b* and *c*). To our surprise, however, we found that the isolated N-terminal domain (residues 23–119), which includes both of the putative ADDL-binding sites, had no effect on polymerization (Fig. 6*d*). A more C-terminally extended construct, 23–144, which ends just before the first α-helix, had a weak inhibitory effect at the highest concentrations, but much less than full-length PrP(23–230) (Fig. 6*e*). Taken together, these results imply that both the N-terminal and C-terminal domains of PrP are required for efficient inhibition of Aβ fibril elongation. We also tested a construct (Δ105–125), which is missing only a short hinge region connecting the N- and C-terminal domains, and found that it inhibited polymerization less effectively than the wild-type protein, implying that this region is also important for inhibitory activity (Fig. 6*f*). Fig. 6*G* summarizes the relative polymerization half-times for each of the PrP constructs.

To determine whether the observed differences in the ability of the PrP constructs to inhibit Aβ polymerization were due to alterations in their binding affinity for Aβ fibrils, we carried out DELFIA-binding assays. Surprisingly, the two C-terminally deleted constructs (23–119 and 23–144), as well as the internally deleted construct (Δ105–125), all of which showed greatly diminished ability to inhibit Aβ polymerization, displayed relatively unimpaired affinity for Aβ fibrils (Fig. 7*a*). In contrast, the 110–230 construct, which is missing the N-terminal, ADDL-binding domains, exhibited significantly reduced binding to fibrils. These results imply that fibril binding, like ADDL binding, depends primarily on sites in the N-terminal domain. Importantly, although the C-terminal domain is not required for fibril binding, this domain (along with the hinge region) nevertheless plays a crucial role in the ability of PrP to inhibit fibril elongation.

We also used DELFIA to test the ability of the different PrP constructs to bind to Aβ monomers. Surprisingly, we found that the C-terminally deleted construct 23–119 displayed a greatly reduced ability to bind to Aβ monomers (Fig. 7*b*), although it showed an affinity for fibrils comparable with full-length PrP (Fig. 7*a*). The 23–144 construct displayed slightly reduced monomer binding. As expected, the 110–230 construct exhibited virtually no monomer binding. These results suggest that the C-terminal domain of PrP (particularly resi-

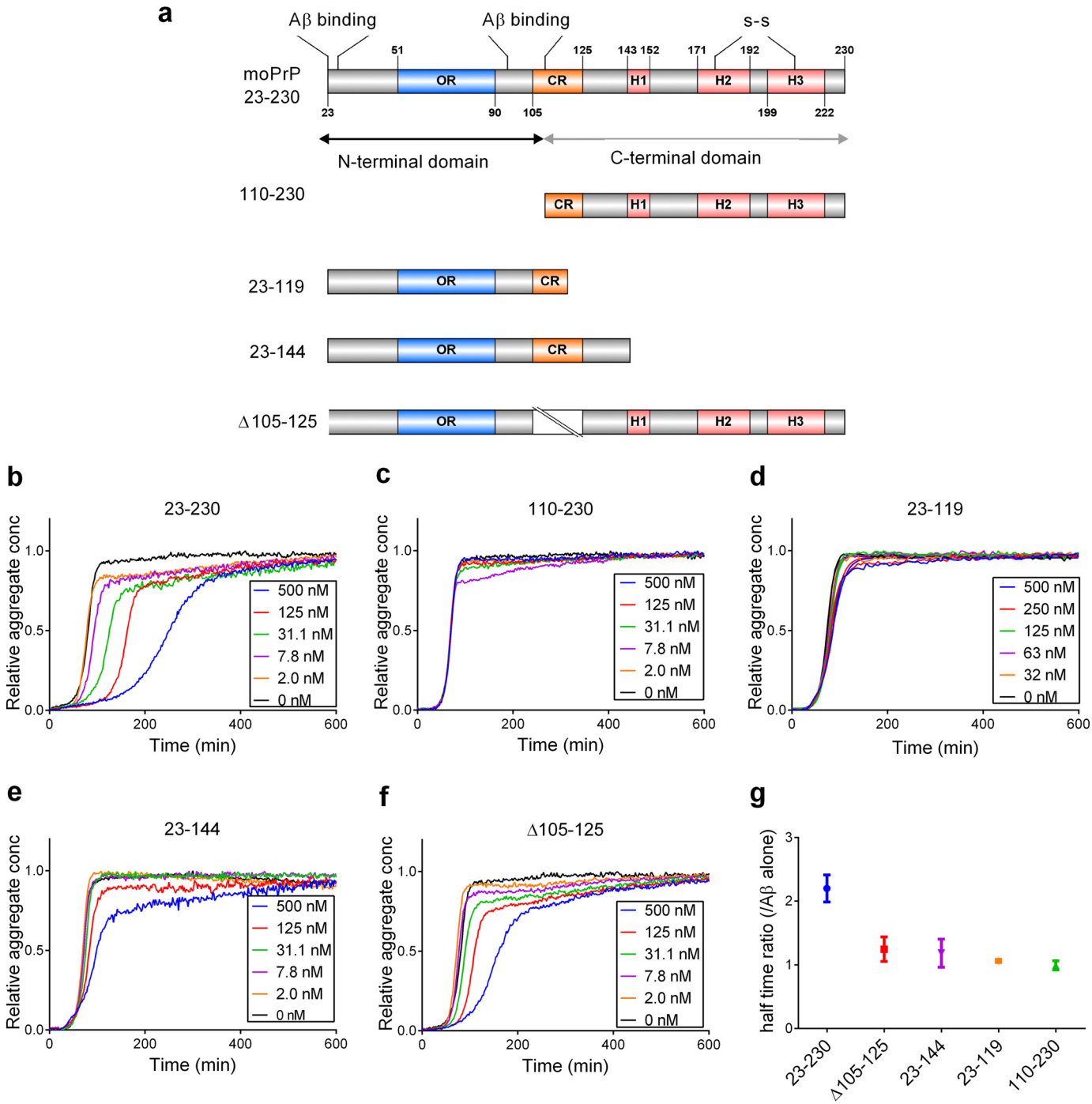

Figure 6. The C-terminal domain of PrP is required for inhibition of Aβ polymerization. *a*, diagrams of the five constructs used for inhibition experiments. The two Aβ-binding sites are indicated on the 23–230 construct. *OR*, octapeptide repeats; *CR*, central region linker (residues 105–125); *H1–H3*, three α-helices in the structured C-terminal domain. *b–f*, ThT curves for polymerization of Aβ (5 μM) in the presence of increasing concentrations of PrP(23–230) (wild type) (*b*), PrP(110–230) (*c*), PrP(23–119) (*d*), PrP(23–144) (*e*), and PrPΔ105–125 (*f*). *g*, polymerization half-times for the indicated PrP constructs at a concentration of 125 nM, expressed as a ratio to the half-time in the absence of PrP. *Symbols* represent the mean of three replicates with S.E.

dues 120–144) influences binding to Aβ monomers, although this region is not essential for binding to Aβ fibrils.

Discussion

There has been considerable interest in the unexpected ability of PrP^C to bind Aβ aggregates (5–8), both because of evidence that PrP^C may transduce some of the neurotoxic effects of such aggregates in AD (9–13) and because of the possibility that exogenous PrP or anti-PrP antibodies could be used as therapeutic agents to neutralize such toxic effects (14–16, 33). Whereas many previous studies have focused on binding of PrP to heterogeneous preparations of soluble oligomers (ADDLs), we have characterized the effect of PrP on the polymerization of Aβ under highly reproducible conditions in which conversion of monomeric to fibrillar forms proceeds via a series of kinetically well-characterized steps, including primary nucleation,

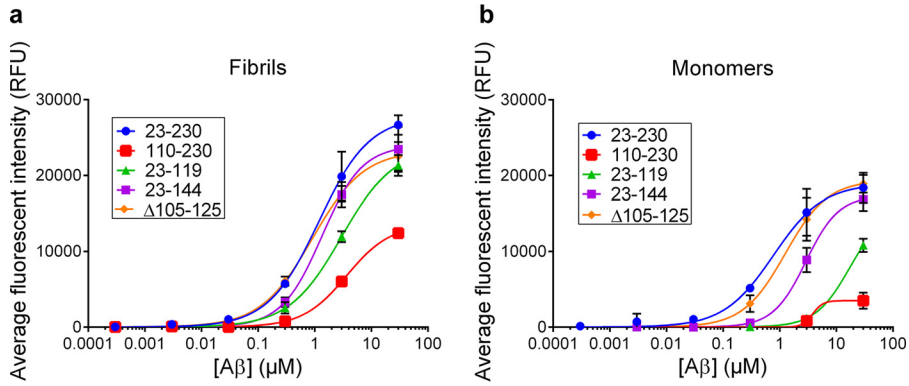

Figure 7. Deletion of the C-terminal domain of PrP has little effect on its binding to Aβ fibrils but reduces its binding to Aβ monomers. *a* and *b*, DELFIA assays of binding of Aβ fibrils (polymerized for 16 h) (*a*) or Aβ monomers (purified by SEC) (*b*) to the indicated PrP constructs. The concentrations of Aβ in monomer equivalents are shown on the *x* axis. Average fluorescence intensity was corrected for background binding of Aβ to wells without PrP. *RFU*, relative fluorescence units.

secondary nucleation, and elongation (22–24). Our results have allowed us to pinpoint which of these steps is inhibited by PrP, as well as which Aβ species and molecular sites PrP is likely to bind. Our study has implications for understanding the neurotoxicity of Aβ oligomers, and it suggests new approaches to targeting PrP for therapeutic purposes in AD.

Taken together, our results suggest a molecular model in which PrP binds tightly to the ends of growing fibrils, specifically inhibiting the elongation step of fibril growth (Fig. 8*a*). This mechanism is supported by several pieces of evidence. Most importantly, it provides an extremely close fit of the ThT polymerization curves to published differential equations (22, 25–27) describing the kinetics of Aβ polymerization. In this scheme, the data are best modeled by assuming that PrP specifically reduces k_+, the rate constant for fibril elongation, and that it does so by binding to fibril ends with an equilibrium dissociation constant, K_d, in the nanomolar range. In contrast, models based on inhibition of primary or secondary nucleation result in very poor fits to the data. The model shown in Fig. 8*a* is also consistent with the substoichiometric nature of PrP inhibition, because only 1–2 PrP molecules would need to bind to each fibril to completely block elongation. This mechanism is also consistent with our observation that PrP has relatively little effect on seeded polymerization, which depends strongly on secondary nucleation. In contrast, chaperones that inhibit secondary nucleation of Aβ dramatically retard seeded polymerization reactions (28). Finally, we have demonstrated, using several different techniques (SPR, DELFIA, FP), that PrP binds to fibrillar Aβ, as would be predicted by this model. Although the K_d for this interaction is difficult to calculate from our data due to uncertainty in the actual concentration of fibrils being analyzed, it is likely to be in the submicromolar range, consistent with the value arrived at from the kinetic modeling.

We have made the unexpected observation that fragments of PrP encompassing only the N-terminal domain show a greatly reduced ability to inhibit Aβ polymerization, although their affinity for Aβ fibrils is relatively unaltered. Our data demonstrate that the N-terminal domain of PrP, encompassing the two previously described ADDL-binding sites, is essential for binding to fibrils but that this interaction alone is insufficient to block elongation. Rather, an additional involvement of the globular C-terminal domain is required. Because the globular domain itself lacks significant fibril-binding activity, the question arises as to how this domain contributes to elongation inhibition. One possibility is that binding of the N-terminal domain positions the C-terminal domain in proximity to the fibril end, sterically blocking access of additional Aβ subunits. Alternatively, binding of Aβ to the N-terminal domain of PrP may cause a conformational change in the C-terminal domain that unmasks additional Aβ-binding sites in that region. We have found that deletion of a short hinge region (residues 105–125) linking the N- and C-terminal domains impairs the ability of PrP to inhibit polymerization, consistent with the idea that inhibitory activity depends on interactions between the two domains. NMR experiments support such an interdomain docking mechanism (34). We note that, in a previous study, the C-terminally truncated construct PrP(23–144) was reported to inhibit Aβ polymerization as effectively as full-length PrP (33). In contrast, we found that this construct had significantly reduced inhibitory potency, a discrepancy that could be due to the different polymerization conditions used in the two experiments.

Interestingly, we have found that PrP binds weakly to Aβ monomers, and this binding is diminished when the C-terminal domain of PrP (particularly residues 120–144) is deleted. This observation suggests that the PrP C-terminal domain contributes to recognizing the unstructured conformation of the Aβ monomer. This conformation might be present transiently after a new monomer is added to the end of the growing fibril, before it is locked into the cross-β-structure characteristic of the rest of the fibril (35), thus explaining why C-terminally deleted PrP constructs have reduced ability to inhibit elongation. Alternatively, it is possible that PrP binding to the zero time sample, which we interpret as monomer binding, really represents binding to a minor population of small oligomers or short fibrils that forms rapidly during the time required to carry out the DELFIA assay. In any case, the fact that PrP inhibits Aβ polymerization at substoichiometric ratios makes it unlikely that it acts primarily by binding to Aβ monomers. Previous studies have documented binding of PrP to Aβ fibrils as well as to ADDLs, although PrP has generally been said to lack affinity for Aβ monomers (5, 6). However, weak binding of PrP to mono-

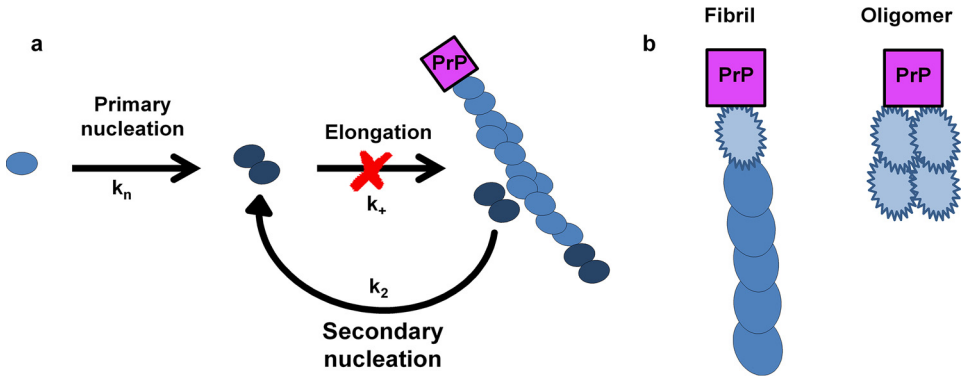

Figure 8. Model for the inhibitory effect of PrP on Aβ polymerization and a possible mechanism for PrP interaction with toxic Aβ oligomers. *a*, *schematic* showing the individual steps in the Aβ polymerization process, with corresponding rate constants. PrP binds to the ends of growing filaments, blocking elongation by reducing k_+. *b*, PrP recognizes structural features common to fibril ends and oligomers.

mers has been observed in some cases (15), consistent with the results presented here.

Previous studies have identified several other proteins that act as chaperones affecting particular steps in the polymerization of Aβ or other amyloidogenic proteins (23). For example, DNAJB6 has been shown to block primary nucleation of Aβ by specifically targeting small oligomers (36), and proSP-C BRICHOS inhibits secondary nucleation by binding stoichiometrically along the surface of Aβ fibrils (28). A particularly relevant example is Ssa1, an Hsp70-type chaperone that blocks elongation of fibrils formed by the yeast prion protein, Ure2p, most likely by binding to fibril ends (37). The kinetic features of Ssa1 inhibition of Ure2p polymerization, based on ThT curves, are strikingly similar to those of PrP inhibition of Aβ polymerization described here, consistent with the conclusion that both proteins inhibit fibril elongation by binding to fibril ends. In contrast, the ThT curves for Aβ polymerization in the presence of PrP and DNAJB6 are quite distinct from each other, arguing that PrP does not target the small population of oligomers that forms transiently during the reaction.

Many previous studies have reported that PrP^C binds tightly and specifically to ADDLs (5–8). This observation has received considerable attention because ADDLs have been shown to have neurotoxic effects, such as suppression of long-term potentiation and retraction of dendritic spines (4, 5). Thus, it has been proposed that PrP^C may serve as a cell-surface receptor that binds Aβ oligomers and mediates their neurotoxic effects in the context of AD. What is the relationship between the ability of PrP^C to bind ADDLs and its ability, demonstrated here, to bind to the ends of growing Aβ fibrils and inhibit elongation? ADDLs are clearly distinct from the Aβ fibrils that we generate in our experiments, in terms of their smaller size, their globular morphology, their much lower ThT-binding capacity, and their inability to seed polymerization when added to monomeric Aβ (not shown). Although often described as being oligomeric, ADDLs also appear to be different from the smaller oligomers (<100 kDa) that have been shown to accumulate transiently and at low levels (<1% of total Aβ) when polymerization is performed under the conditions we have used here (22). Despite these differences, however, PrP may bind strongly to ADDLs because they display some of the same structural features as fibril ends (Fig. 8*b*). Perhaps ADDLs represent Aβ assemblies that are trapped in an elongation-ready mode capable of binding PrP. Although ADDLs do not seem to evolve to a fibrillar state, there is evidence that their morphology can change over time, with the appearance of nanotubular structures that have potent neurotoxicity and bind avidly to PrP^C (8).

Our results have important implications for theories of how Aβ causes neurotoxicity in AD. Considerable evidence indicates that Aβ oligomers, rather than fibrils or monomers, have the greatest neurotoxic potency *in vivo* as well as in cell-based assays (2). The data presented here suggest that this may reflect structural features common to both oligomers and fibril ends and the ability of PrP^C and perhaps other cell-surface receptors to recognize these features. According to this hypothesis, small, soluble assemblies of Aβ, including oligomers, protofibrils, or nanotubes, may present a high molar concentration of protein surfaces that are structurally equivalent to fibril ends and that can therefore bind to and activate PrP^C or other toxicity-transducing receptors on the neuronal surface. Consistent with this theory, structural studies suggest that Aβ fibril ends and toxic oligomers both display β-strands with dangling hydrogen bonds, which are not connected to sites on adjacent strands (35, 38). Oligomer-specific antibodies are capable of recognizing such structures (39, 40), and perhaps PrP^C may do the same. It is also interesting to speculate that PrP^C, which is a relatively abundant and widely distributed cell-surface protein on both neurons and glia, might influence the polymerization of Aβ within the brain, inhibiting elongation and contributing to the accumulation of soluble, neurotoxic assemblies.

It has been proposed that small-molecule ligands that bind to PrP^C and prevent interaction with Aβ oligomers could represent useful therapeutic agents for treatment of AD (41). However, pharmacologically targeting the N-terminal domain of PrP^C, which contains the major Aβ-binding sites, is problematic, because this region is flexibly disordered, and does not present well-defined pockets for binding small molecules. In addition, ligands that interact with the N-terminal domain could produce adverse side effects, because this region has been shown to play a role in certain physiological activities of PrP^C, such as neuronal development and cell adhesion (42, 43). Our data raise the possibility that small-molecule ligands for the globular C-terminal domain of PrP, which is in principle more druggable, may specifically antagonize secondary interactions

with oligomeric or fibrillar Aβ. If so, these ligands might provide superior tools for preventing Aβ neurotoxicity.

Experimental procedures

Preparation of Aβ monomers and ADDLs

Lyophilized Aβ 1–42 was purchased from the ERI Amyloid Laboratory, LLC (Oxford, CT). The peptide was solubilized in water, and one volumetric equivalent acetonitrile was added as a cryoprotectant before the solubilized peptide was separated into 1-mg aliquots, lyophilized, and stored at −80 °C until use. For monomer preparation, the peptide was solubilized in 15 mM NaOH as described previously (44) without the addition of TCEP. Monomers were isolated by size-exclusion chromatography on a Superdex 75 10/300 GL (GE Healthcare) column using PBS as the running buffer. Fractions were collected and kept on ice for immediate use in ThT assays or were flash-frozen in liquid nitrogen and stored at −80 °C until needed for EM or binding studies. The concentration of Aβ was estimated with a NanoDrop UV-visible spectrometer (Thermo Scientific) by reading the sample absorbance at 214 nm and applying Beer's law with an extinction coefficient of 76,848 M^{-1} cm^{-1}. ADDLs were prepared using a standard protocol (45, 46) in which lyophilized Aβ peptide was solubilized in HFIP and dried to a film. The film was then solubilized in DMSO before dilution to a concentration of 100 μM in Ham's F-12 phenol red–free medium (total DMSO 2% (v/v)), followed by incubation at room temperature for 16 h. For seeding assays, Aβ monomers were incubated for 16 h in PBS at 37 °C, with or without 500 nM PrP. Fibril seeds were sonicated on ice for 10 min on 50% duty cycle before use.

ThT assay for Aβ polymerization

Kinetic assays for Aβ polymerization were conducted as described previously (22, 29). Briefly, monomers of Aβ were diluted to a concentration of 3–10 μM in PBS, and 10 μM ThT was added from a stock of 1 mM. Recombinant PrP was added from a 1 mg/ml stock in water at the indicated concentrations. To follow ThT binding, 100-μl samples were added to 96-well, half-volume, low-binding plates (Corning 3881), and florescence was read in a Synergy H1 multimode microplate reader (BioTek) every 2 or 6 min at 37 °C (excitation 440 nm, emission 480 nm). Samples used for binding studies were removed directly from the wells and transferred to low-binding, 1.5-ml tubes, flash-frozen, and stored at −80 °C until use.

Recombinant PrP

Full-length mouse PrP(23–230) and PrP(23–109)-cys sequences were synthesized by ATUM/DNA 2.0 (Newark, CA) in the vectors pJ414 and pJ411, respectively, using *Escherichia coli*–optimized codons, and were then subcloned into the pET101 vector using the Champion pET101 Directional TOPO expression kit (Invitrogen). The deletion variants were generated by site-directed mutagenesis using appropriate primers, and PrP(23–230) as the template. All constructs were verified by DNA sequencing. The pET101 vector was then transformed into BL21 Star chemically competent *E. coli* and expressed for 16 h via autoinduction (47). All constructs were expressed and purified as described previously (48), with minor modifications as follows. Cells were lysed, and inclusion bodies containing PrP(23–230), 23–230–c-Myc, Δ105–125, or His_6-TEV-110–230 were purified from the lysate. In the case of the N-terminal constructs 23–119, 23–109-cys, and 23–144, no inclusion body purification was required, and lysis buffer did not contain chaotropic agents. All constructs were then purified with an ÄKTA purification system (GE Healthcare) using a Ni^{2+}-immobilized metal ion affinity column. For the construct 23–109-cys, 1 mM TCEP was added to all Ni^{2+} buffers to prevent oxidation of the C-terminal cysteine. Protein was eluted from the Ni^{2+} immobilized metal ion affinity column with 5 M guanidine HCl, 0.1 M Tris acetate, 0.1 M potassium phosphate (pH 4.5) while monitoring A_{280}. Fractions spanning the elution peak were combined, and the pH was raised to 8 by titration with potassium acetate. For full-length PrP(23–230) as well as PrPΔ105–125, this was followed by storage at 4 °C overnight to facilitate proper folding. For PrP(110–230), which was expressed with a 5′-His_6 tag and TEV cleavage site (sequence MRGSHHHHH-HGENLYFQG), the eluent from the Ni^{2+} column was desalted into 20 mM Tris, 20 mM KOAc, pH 8.0, and 0.1 mg of TEV protease was added. Enzymatic cleavage was allowed to proceed overnight at 4 °C. The TEV protease was removed the following day with Ni^{2+} resin, and the remaining protein was concentrated and purified using the Superdex 75 10/300 GL column in 20 mM Tris, 20 mM KOAc, pH 8.0. The protein was flash-frozen in this buffer and stored at −80 °C until use. All other constructs were desalted using a HiPrep 26/10 desalting column (GE Healthcare) into 20 mM potassium acetate, pH 5.5, and then purified by reverse-phase HPLC using a C4 column (Grace/Vydac). Fractions containing the purified protein were pooled, lyophilized, and stored at −80 °C for future use. Protein stocks were reconstituted in 0.2-μm filtered water and quantified with a NanoDrop UV-visible spectrometer (Thermo Scientific) before use. The sequence for the 3′-c-Myc tag was EQKLISEEDL.

Alexa Fluor 488-labeled mouse PrP(23–109)

Alexa Fluor 488 C_5 maleimide (Thermo Fisher Scientific) was dissolved in water at a stock concentration of 1 mM. Lyophilized 23–109-cys (N1-cys) was dissolved in 20 mM MOPS, pH 7.4, and 0.5 mM TCEP to a concentration of 100 μM, and Alexa Fluor 488 was added dropwise with stirring to a final ratio of 1:1, giving a final concentration of 50 μM N1-cys, 500 μM Alexa Fluor 488. This solution was protected from light and allowed to incubate at room temperature for 2 h on a benchtop rotator. After 2 h, 1 ml of the solution was injected into an analytical C3 column (Zorbax 300SB C3, Agilent) on an Agilent 1200 Infinity HPLC system, and the peptide peak was collected and lyophilized. Confirmation of successful linkage was made by MALDI-TOF mass spectrometry.

Analytical SEC

Analysis of monomer depletion during Aβ polymerization was performed using an Agilent Bio Sec-3 300 Å column running in PBS on an Agilent 1200 Infinity HPLC system. Aβ samples were spun down at 16,000 rpm in a benchtop centrifuge

and filtered with a 0.2-μm filter to remove insoluble aggregates before injecting 500 μl onto the column.

Circular dichroism

Far-UV spectra (193–250 nm, 1-nm bandwidth) were collected at 37 °C from samples of 20 μM Aβ that had been polymerized for different times using a Jasco J-815 spectropolarimeter (Jasco, Inc.) with a 1-mm path length quartz cell. Raw data (in millidegrees) were converted to mean residue ellipticity using a molecular mass for Aβ(1–42) of 4514.1 Da.

Electron microscopy

To prepare fibrils for imaging, samples of Aβ were spun down at 100,000 × *g* in a TLA 55 fixed-angle rotor (Beckman Coulter) for 30 min. The initial sample volume was 900 μl. 890 μl of the supernatant was removed before diluting the remaining sample 1:2 in ultrapure water. The sample was applied as a 4.5-μl droplet to a glow-discharged, 300-mesh copper grid and allowed to incubate for 4 min before washing 12 times with filtered, ultrapure water. The grid surface was then stained for 1 min in 2% uranyl acetate and dried for 3 min. Images were taken using a Philips CM12 120KV transmission microscope. Scale bars were added to images, and measurements of fibrils were made using ImageJ, with each reported size representing an average of 30 independent measurements.

Semidenaturing detergent-agarose gel electrophoresis

SDD-AGE of Aβ fibrils was performed as described previously (49). The gel was prepared with 1.5% agarose in Tris acetate buffer (25 mM Tris acetate, pH 8.5, 250 mM glycine, 0.1% SDS). Samples were not boiled after Laemmli loading buffer was added to avoid further aggregation. The gel was allowed to run for 4 h at 100 mV at 4 °C to achieve best separation of samples. The samples were capillary-transferred overnight to a 0.2-μm PVDF membrane in Tris acetate buffer with 20% MeOH. Membranes were blocked overnight in 3% (w/v) BSA in TBST before immunoprobing with 6E10 anti-Aβ mouse IgG (BioLegend) and anti-mouse IgG (Sigma).

Surface plasmon resonance (SPR)

SPR was performed using the ProteOn XPR36 protein interaction array system (Bio-Rad) as described previously (7). 9E10 anti-c-Myc antibody (Invitrogen) was immobilized on a ProteOn GLM sensor chip using the standard protocol for amine coupling. PrP(23–230)-c-Myc (ligand) was captured on the surface, followed by an analyte flow step with Aβ monomers, fibrils, or ADDLs (injection period 240 s, 50 μl/min flow rate). Nonspecific binding interactions between Aβ and the 9E10 antibody were subtracted from the sensorgram using the ProteOn analysis software.

Dissociation-enhanced lanthanide fluorescence immunoassay (DELFIA)

To coat 96-well DELFIA yellow plates (PerkinElmer Life Sciences), PrP was diluted to 100 nM in 20 mM MOPS, pH 7.4, and 50 μl was added to each well. The plate was incubated for 1 h while shaking at 400 rpm on a Thermomixer R incubator (Eppendorf), and then the wells were washed five times with 300 μl of TBS with 0.05% Tween 20 (TBST). The plates were blocked for 1 h with 0.1% BSA in TBST, followed by another wash step. ADDLs were diluted in PBS, 50 μl was added to each well, and the plate was incubated at 400 rpm for 1 h and then washed. For Aβ time points, samples at each time point were diluted in PBS, and 50 μl was added to each well before incubating the plate for 10 min. Plates were washed, and anti-Aβ antibody 6E10, diluted in DELFIA assay buffer (PerkinElmer Life Sciences), was added at a concentration of 1 μg/ml and incubated for 1 h, followed by another wash. Secondary antibody (DELFIA Eu-N1 anti-mouse IgG, PerkinElmer Life Sciences) was added at a concentration of 0.3 μg/ml and incubated for 1 h. Plates were washed, and DELFIA enhancement solution (PerkinElmer Life Sciences) was added at 100 μl/well and incubated for 15 min before time-resolved fluorescence was measured in a Synergy H1 multi-mode microplate reader (BioTek) (excitation 320 nm; emission 615 nm, 100-ns delay).

Fluorescence polarization

Fluorescently labeled PrP(23–109) was mixed with Aβ samples in PBS. Fluorescent polarization was measured on a Synergy H1 multimode microplate reader fitted with a Green FP (485/528) filter cube (BioTek). Polarization values were calculated using the Synergy Gen 5 software (BioTek).

Author contributions—D. A. H. and E. B.-F. conceived and coordinated the study and wrote the paper. E. B.-F. designed, performed, and analyzed the experiments and results shown in all figures with the exception of Fig. 4. R. U. and J. E. S. designed and performed the analysis shown in Fig. 4 and supplemental Tables 1 and 2, wrote the supplemental material describing the mathematical analysis, and contributed to the interpretation of the results. All authors reviewed the results and approved the final version of the manuscript.

Acknowledgments—We thank Alex McDonald for providing some of the vectors used to make the PrP constructs. We also thank Don Gantz for assistance with the electron microscopy and development of the images in Fig. 1 and Elena Klimtchuk, who assisted in collecting the CD curves.

References

1. Selkoe, D. J. (2011) Alzheimer's disease. *Cold Spring Harb. Perspect. Biol.* 10.1101/cshperspect.a004457
2. Walsh, D. M., and Selkoe, D. J. (2007) Aβ oligomers: a decade of discovery. *J. Neurochem.* **101,** 1172–1184
3. Shankar, G. M., Li, S., Mehta, T. H., Garcia-Munoz, A., Shepardson, N. E., Smith, I., Brett, F. M., Farrell, M. A., Rowan, M. J., Lemere, C. A., Regan, C. M., Walsh, D. M., Sabatini, B. L., and Selkoe, D. J. (2008) Amyloid-β protein dimers isolated directly from Alzheimer's brains impair synaptic plasticity and memory. *Nat. Med.* **14,** 837–842
4. Lacor, P. N., Buniel, M. C., Furlow, P. W., Clemente, A. S., Velasco, P. T., Wood, M., Viola, K. L., and Klein, W. L. (2007) Aβ oligomer-induced aberrations in synapse composition, shape, and density provide a molecular basis for loss of connectivity in Alzheimer's disease. *J. Neurosci.* **27,** 796–807
5. Laurén, J., Gimbel, D. A., Nygaard, H. B., Gilbert, J. W., and Strittmatter, S. M. (2009) Cellular prion protein mediates impairment of synaptic plasticity by amyloid-β oligomers. *Nature* **457,** 1128–1132
6. Chen, S., Yadav, S. P., and Surewicz, W. K. (2010) Interaction between human prion protein and amyloid-β (Aβ) oligomers: the role of N-terminal residues. *J. Biol. Chem.* **285,** 26377–26383

7. Fluharty, B. R., Biasini, E., Stravalaci, M., Sclip, A., Diomede, L., Balducci, C., La Vitola, P., Messa, M., Colombo, L., Forloni, G., Borsello, T., Gobbi, M., and Harris, D. A. (2013) An N-terminal fragment of the prion protein binds to amyloid-β oligomers and inhibits their neurotoxicity *in vivo*. *J. Biol. Chem.* **288,** 7857–7866
8. Nicoll, A. J., Panico, S., Freir, D. B., Wright, D., Terry, C., Risse, E., Herron, C. E., O'Malley, T., Wadsworth, J. D., Farrow, M. A., Walsh, D. M., Saibil, H. R., and Collinge, J. (2013) Amyloid-β nanotubes are associated with prion protein-dependent synaptotoxicity. *Nat. Commun.* **4,** 2416
9. Um, J. W., Kaufman, A. C., Kostylev, M., Heiss, J. K., Stagi, M., Takahashi, H., Kerrisk, M. E., Vortmeyer, A., Wisniewski, T., Koleske, A. J., Gunther, E. C., Nygaard, H. B., and Strittmatter, S. M. (2013) Metabotropic glutamate receptor 5 is a coreceptor for Alzheimer Aβ oligomer bound to cellular prion protein. *Neuron* **79,** 887–902
10. Um, J. W., Nygaard, H. B., Heiss, J. K., Kostylev, M. A., Stagi, M., Vortmeyer, A., Wisniewski, T., Gunther, E. C., and Strittmatter, S. M. (2012) Alzheimer amyloid-β oligomer bound to postsynaptic prion protein activates Fyn to impair neurons. *Nat. Neurosci.* **15,** 1227–1235
11. Haas, L. T., Kostylev, M. A., and Strittmatter, S. M. (2014) Therapeutic molecules and endogenous ligands regulate the interaction between brain cellular prion protein (PrP^C) and metabotropic glutamate receptor 5 (mGluR5). *J. Biol. Chem.* **289,** 28460–28477
12. Haas, L. T., and Strittmatter, S. M. (2016) Oligomers of amyloid β prevent physiological activation of the cellular prion protein-metabotropic glutamate receptor 5 complex by glutamate in Alzheimer disease. *J. Biol. Chem.* **291,** 17112–17121
13. Gimbel, D. A., Nygaard, H. B., Coffey, E. E., Gunther, E. C., Laurén, J., Gimbel, Z. A., and Strittmatter, S. M. (2010) Memory impairment in transgenic Alzheimer mice requires cellular prion protein. *J. Neurosci.* **30,** 6367–6374
14. Klyubin, I., Nicoll, A. J., Khalili-Shirazi, A., Farmer, M., Canning, S., Mably, A., Linehan, J., Brown, A., Wakeling, M., Brandner, S., Walsh, D. M., Rowan, M. J., and Collinge, J. (2014) Peripheral administration of a humanized anti-PrP antibody blocks Alzheimer's disease Aβ synaptotoxicity. *J. Neurosci.* **34,** 6140–6145
15. Freir, D. B., Nicoll, A. J., Klyubin, I., Panico, S., Mc Donald, J. M., Risse, E., Asante, E. A., Farrow, M. A., Sessions, R. B., Saibil, H. R., Clarke, A. R., Rowan, M. J., Walsh, D. M., and Collinge, J. (2011) Interaction between prion protein and toxic amyloid β assemblies can be therapeutically targeted at multiple sites. *Nat. Commun.* **2,** 336
16. Chung, E., Ji, Y., Sun, Y., Kascsak, R. J., Kascsak, R. B., Mehta, P. D., Strittmatter, S. M., and Wisniewski, T. (2010) Anti-PrP^C monoclonal antibody infusion as a novel treatment for cognitive deficits in an Alzheimer's disease model mouse. *BMC Neurosci.* **11,** 130
17. Balducci, C., Beeg, M., Stravalaci, M., Bastone, A., Sclip, A., Biasini, E., Tapella, L., Colombo, L., Manzoni, C., Borsello, T., Chiesa, R., Gobbi, M., Salmona, M., and Forloni, G. (2010) Synthetic amyloid-β oligomers impair long-term memory independently of cellular prion protein. *Proc. Natl. Acad. Sci. U.S.A.* **107,** 2295–2300
18. Calella, A. M., Farinelli, M., Nuvolone, M., Mirante, O., Moos, R., Falsig, J., Mansuy, I. M., and Aguzzi, A. (2010) Prion protein and Aβ-related synaptic toxicity impairment. *EMBO Mol. Med.* **2,** 306–314
19. Cissé, M., Sanchez, P. E., Kim, D. H., Ho, K., Yu, G. Q., and Mucke, L. (2011) Ablation of cellular prion protein does not ameliorate abnormal neural network activity or cognitive dysfunction in the J20 line of human amyloid precursor protein transgenic mice. *J. Neurosci.* **31,** 10427–10431
20. Kessels, H. W., Nguyen, L. N., Nabavi, S., and Malinow, R. (2010) The prion protein as a receptor for amyloid-β. *Nature* **466,** E3–E4; discussion E4–E5
21. Lambert, M. P., Barlow, A. K., Chromy, B. A., Edwards, C., Freed, R., Liosatos, M., Morgan, T. E., Rozovsky, I., Trommer, B., Viola, K. L., Wals, P., Zhang, C., Finch, C. E., Krafft, G. A., and Klein, W. L. (1998) Diffusible, nonfibrillar ligands derived from $Aβ_{1-42}$ are potent central nervous system neurotoxins. *Proc. Natl. Acad. Sci. U.S.A.* **95,** 6448–6453
22. Cohen, S. I., Linse, S., Luheshi, L. M., Hellstrand, E., White, D. A., Rajah, L., Otzen, D. E., Vendruscolo, M., Dobson, C. M., and Knowles, T. P. (2013) Proliferation of amyloid-β42 aggregates occurs through a secondary nucleation mechanism. *Proc. Natl. Acad. Sci. U.S.A.* **110,** 9758–9763
23. Arosio, P., Michaels, T. C., Linse, S., Månsson, C., Emanuelsson, C., Presto, J., Johansson, J., Vendruscolo, M., Dobson, C. M., and Knowles, T. P. (2016) Kinetic analysis reveals the diversity of microscopic mechanisms through which molecular chaperones suppress amyloid formation. *Nat. Commun.* **7,** 10948
24. Cohen, S. I., Vendruscolo, M., Dobson, C. M., and Knowles, T. P. (2012) From macroscopic measurements to microscopic mechanisms of protein aggregation. *J. Mol. Biol.* **421,** 160–171
25. Cohen, S. I., Vendruscolo, M., Dobson, C. M., and Knowles, T. P. (2011) Nucleated polymerization with secondary pathways. III. Equilibrium behavior and oligomer populations. *J. Chem. Phys.* **135,** 065107
26. Cohen, S. I., Vendruscolo, M., Dobson, C. M., and Knowles, T. P. (2011) Nucleated polymerization with secondary pathways. II. Determination of self-consistent solutions to growth processes described by non-linear master equations. *J. Chem. Phys.* **135,** 065106
27. Cohen, S. I., Vendruscolo, M., Welland, M. E., Dobson, C. M., Terentjev, E. M., and Knowles, T. P. (2011) Nucleated polymerization with secondary pathways. I. Time evolution of the principal moments. *J. Chem. Phys.* **135,** 065105
28. Cohen, S. I., Arosio, P., Presto, J., Kurudenkandy, F. R., Biverstal, H., Dolfe, L., Dunning, C., Yang, X., Frohm, B., Vendruscolo, M., Johansson, J., Dobson, C. M., Fisahn, A., Knowles, T. P., and Linse, S. (2015) A molecular chaperone breaks the catalytic cycle that generates toxic Aβ oligomers. *Nat. Struct. Mol. Biol.* **22,** 207–213
29. Hellstrand, E., Boland, B., Walsh, D. M., and Linse, S. (2010) Amyloid β-protein aggregation produces highly reproducible kinetic data and occurs by a two-phase process. *ACS Chem. Neurosci.* **1,** 13–18
30. Arosio, P., Cukalevski, R., Frohm, B., Knowles, T. P., and Linse, S. (2014) Quantification of the concentration of Aβ42 propagons during the lag phase by an amyloid chain reaction assay. *J. Am. Chem. Soc.* **136,** 219–225
31. Arosio, P., Knowles, T. P., and Linse, S. (2015) On the lag phase in amyloid fibril formation. *Phys. Chem. Chem. Phys.* **17,** 7606–7618
32. Willander, H., Presto, J., Askarieh, G., Biverstål, H., Frohm, B., Knight, S. D., Johansson, J., and Linse, S. (2012) BRICHOS domains efficiently delay fibrillation of amyloid β-peptide. *J. Biol. Chem.* **287,** 31608–31617
33. Nieznanski, K., Choi, J. K., Chen, S., Surewicz, K., and Surewicz, W. K. (2012) Soluble prion protein inhibits amyloid β (Aβ) fibrillization and toxicity. *J. Biol. Chem.* **287,** 33104–33108
34. Wu, B., McDonald, A. J., Markham, K., Rich, C. B., McHugh, K. P., Tatzelt, J., Colby, D. W., Millhauser, G. L., and Harris, D. A. (2017) The N-terminus of the prion protein is a toxic effector regulated by the C-terminus. *Elife* 10.7554/eLife.23473
35. Lührs, T., Ritter, C., Adrian, M., Riek-Loher, D., Bohrmann, B., Döbeli, H., Schubert, D., and Riek, R. (2005) 3D structure of Alzheimer's amyloid-β(1–42) fibrils. *Proc. Natl. Acad. Sci. U.S.A.* **102,** 17342–17347
36. Månsson, C., Arosio, P., Hussein, R., Kampinga, H. H., Hashem, R. M., Boelens, W. C., Dobson, C. M., Knowles, T. P., Linse, S., and Emanuelsson, C. (2014) Interaction of the molecular chaperone DNAJB6 with growing amyloid-β42 (Aβ42) aggregates leads to sub-stoichiometric inhibition of amyloid formation. *J. Biol. Chem.* **289,** 31066–31076
37. Xu, L. Q., Wu, S., Buell, A. K., Cohen, S. I., Chen, L. J., Hu, W. H., Cusack, S. A., Itzhaki, L. S., Zhang, H., Knowles, T. P., Dobson, C. M., Welland, M. E., Jones, G. W., and Perrett, S. (2013) Influence of specific HSP70 domains on fibril formation of the yeast prion protein Ure2. *Philos. Trans. R. Soc. Lond. B Biol. Sci.* **368,** 20110410
38. Liu, C., Zhao, M., Jiang, L., Cheng, P. N., Park, J., Sawaya, M. R., Pensalfini, A., Gou, D., Berk, A. J., Glabe, C. G., Nowick, J., and Eisenberg, D. (2012) Out-of-register β-sheets suggest a pathway to toxic amyloid aggregates. *Proc. Natl. Acad. Sci. U.S.A.* **109,** 20913–20918
39. Kayed, R., Head, E., Thompson, J. L., McIntire, T. M., Milton, S. C., Cotman, C. W., and Glabe, C. G. (2003) Common structure of soluble amyloid oligomers implies common mechanism of pathogenesis. *Science* **300,** 486–489
40. Liu, P., Reed, M. N., Kotilinek, L. A., Grant, M. K., Forster, C. L., Qiang, W., Shapiro, S. L., Reichl, J. H., Chiang, A. C., Jankowsky, J. L., Wilmot, C. M., Cleary, J. P., Zahs, K. R., and Ashe, K. H. (2015) Quaternary structure defines a large class of amyloid-β oligomers neutralized by sequestration. *Cell Rep.* **11,** 1760–1771

41. Biasini, E., and Harris, D. A. (2012) Targeting the cellular prion protein to treat neurodegeneration. *Future Med. Chem.* **4,** 1655–1658
42. Santuccione, A., Sytnyk, V., Leshchyns'ka, I., and Schachner, M. (2005) Prion protein recruits its neuronal receptor NCAM to lipid rafts to activate p59fyn and to enhance neurite outgrowth. *J. Cell Biol.* **169,** 341–354
43. Slapšak, U., Salzano, G., Amin, L., Abskharon, R. N., Ilc, G., Zupančič, B., Biljan, I., Plavec, J., Giachin, G., and Legname, G. (2016) The N terminus of the prion protein mediates functional interactions with the neuronal cell adhesion molecule (NCAM) fibronectin domain. *J. Biol. Chem.* **291,** 21857–21868
44. Lee, J., Culyba, E. K., Powers, E. T., and Kelly, J. W. (2011) Amyloid-β forms fibrils by nucleated conformational conversion of oligomers. *Nat. Chem. Biol.* **7,** 602–609
45. Klein, W. L. (2002) Aβ toxicity in Alzheimer's disease: globular oligomers (ADDLs) as new vaccine and drug targets. *Neurochem. Int.* **41,** 345–352
46. Stine, W. B., Jungbauer, L., Yu, C., and LaDu, M. J. (2011) Preparing synthetic Aβ in different aggregation states. *Methods Mol. Biol.* **670,** 13–32
47. Studier, F. W. (2005) Protein production by auto-induction in high density shaking cultures. *Protein Expr. Purif.* **41,** 207–234
48. McDonald, A. J., Dibble, J. P., Evans, E. G., and Millhauser, G. L. (2014) A new paradigm for enzymatic control of α-cleavage and β-cleavage of the prion protein. *J. Biol. Chem.* **289,** 803–813
49. Halfmann, R., and Lindquist, S. (2008) Screening for amyloid aggregation by semi-denaturing detergent-agarose gel electrophoresis. *J. Vis. Exp.* 10.3791/838

SUPPLEMENTAL DATA FOR

The prion protein targets amyloid-beta fibrils ends via its C-terminal domain to prevent elongation

Erin Bove-Fenderson[1], Ryo Urano[2], John E. Straub[2], and David A. Harris[1]

From the [1]Department of Biochemistry, Boston University School of Medicine, Boston, MA 02118, and [2]Department of Chemistry, Boston University, Boston, MA 02215

Running title: The prion protein prevents amyloid-beta fibril elongation

Master Equation Analysis

An approximate analytical master equation for protein aggregation including a secondary nucleation pathway was proposed by Cohen et al.(1-3). An alternative master equation including fragmentation rather than secondary nucleation was also proposed but is not considered here, as experiments were conducted under quiescent conditions. The integrated rate law for the normalized fibril mass (total mass excluding monomer mass), M(t), is given by

$$\frac{M(t)}{M(\infty)} = 1 - \left(\frac{B_+C_+}{B_+ + C_+e^{\kappa t}}\frac{B_- + C_+e^{\kappa t}}{B_- + C_+}\right)^{\frac{k_\infty^2}{\kappa\tilde{k}_\infty}} e^{-k_\infty t}, \quad (1)$$

where

$$B_\pm = \frac{k_\infty \pm \tilde{k}_\infty}{2\kappa}$$

$$C_\pm = \frac{\pm\lambda^2}{2\kappa^2}$$

$$k_\infty = \sqrt{\frac{2\kappa^2}{n_2(n_2+1)} + \frac{2\lambda^2}{n_c}}$$

$$\tilde{k}_\infty = \sqrt{k_\infty^2 - 4C_+C_-\kappa^2},$$

assuming $M(0) = 0$ and the initial concentration of fibril $P(0) = 0$ (4). The model parameters can be reduced to two independent degrees of freedom captured by the parameters

$$\lambda = \sqrt{2m(0)^{n_c}k_+k_n}$$
$$\kappa = \sqrt{2m(0)^{n_2+1}k_+k_2},$$

where m(0) is the initial concentration of monomer. These two parameters, λ and κ, separately govern the contributions of the primary nucleation pathway and secondary nucleation pathway, respectively.

In the current experiments, the initial concentration of monomer was fixed to be $m(0) = 3\mu M$. Previous work (4) suggests that reasonable values of n_c and n_2 are 2.

The rate constants were first determined by global fitting using a Levenberg−Marquardt non-linear least-squares algorithm for inhibitor free conditions. In the global fitting, the function to be minimized is defined as

$$\Delta = \sum_{j}^{n_{exp}} \sum^{t=0} (M_{pred,j}(t) - M_{exp,j}(t))^2,$$

where n_{exp} is the number of independent experimental data points for a given inhibitor concentration, $M_{pred}(t) = M(t)/M(\infty)$ is given by Eq. (1), and $M_{exp}(t)$ is the similarly normalized experimental value.

We first obtained the kinetic rate constants for the inhibitor free condition with the initial values of $k_+ = 3{\times}10^6[1/Ms]$, $k_n = 3{\times}10^{-4}[1/Ms]$, and $k_2 = 1{\times}10^4[1/M^2s]$ from Cohen *et al*.(4). For finite inhibitor concentrations, the global fitting was performed in a systematic manner, changing only a single rate constant at a time while holding other parameters fixed to the inhibitor free values. In this way, Δ was independently minimized for datasets representing each inhibitor concentration.

Stochastic Simulation Analysis

We define stochastic rate constants as a_+, a_2, a_n for elongation, secondary nucleation, and primary nucleation, respectively. Using these constants, kinetic rate coefficients for each process are given by

$$k_{+,0M}(t) = 2a_+ m(t) P^{Tot}(t),$$
$$k_{2,0M}(t) = a_2 m(t)^{n_2} M(t),$$
$$k_{n,0M}(t) = a_n m(t)^{n_c}$$

To model stochastic chemical kinetics in the presence of an inhibitor, two assumptions are required. First, that a sufficient concentration of inhibitor exists, stoichiometric for each unbound protein, and second, that inhibitor binding occurs much faster than the production of new unbound molecules, so that inhibitor binding is assumed to be at equilibrium (5).

The total concentration of fibrils, P^{tot}, included contributions from three species of fibrils including inhibitor-free fibrils, P^0, fibrils bound to one inhibitor at one end, P^1, and fibrils bound to two inhibitors, one at each end, P^2. Considering the equilibrium constant of the inhibitor binding, K_{eqEnd}, mass conservation, concentrations, and rate, we find

$$\begin{aligned}
P^{Tot}(t) &= P^0(t) + P^1(t) + P^2(t) \\
P^2(t) &= K_{eqEnd} C_i^{Tot} P^1(t) \\
P^1(t) &= K_{eqEnd} C_i^{Tot} P^0(t) \\
P^0(t) &= \frac{P^{Tot}(t)}{1 + K_{eqEnd} C_i^{Tot} + (K_{eqEnd} C_i^{Tot})^2} \\
k_+ &= 2 * a_+ P^0(t) + a_+ P^1(t),
\end{aligned}$$

where C_i^{Tot} is the inhibitor concentration.

The ratio of the kinetic rate constant for elongation in the presence, k_+, and absence, $k_{+,\,0M}$, of inhibitor is given by

$$\frac{k_+}{k_{+,\,0M}} = \frac{2P^0(t) + P^1(t)}{2P^{Tot}(t)} = \frac{2 + K_{eqEnd} C_i^{Tot}}{2 + 2K_{eqEnd} C_i^{Tot} + 2(K_{eqEnd} C_i^{Tot})^2} = f(K_{eq})$$

Assuming independent binding on available protein sites, specific binding of the inhibitor to the surface of a fibril results in a Langmuir-type adsorption of the inhibitor to the surface. This provides the amount of deactivated monomer with inhibitor bound, M_{bound}, as

$$M_{bound}(t) = K_{eqSurf} C_i^{Tot}(t)$$

$$k_2 = a_2(M(t) - M_{bound}(t))m(t)^{n_2} = (1 - K_{eqSurf} C_i^{Tot}) a_2 M(t) m(t)^{n_2}$$

$$= k_{2,0M}(1 - K_{eqSurf} C_i^{Tot}).$$

The computational analysis of this set of stochastic equations was performed using R (6-9).

Table S1: Polymerization half-time at each PrP concentration. The half-time,$t_{½}$, of polymerization obtained from fitting rate constants, $\mathbf{M_{pred}(t_{half}) = 0.5}$, is shown for various conditions. To obtain the best fit rate constants, the global fitting was performed in a systematic manner by varying three rate constants from the initial values of Cohen *et al*. (4) above for each condition.

PrP concentration	Half-time (min)
250 nM	361.5
125 nM	198.0
62.5 nM	143.3
31.3 nM	104.1
15.6 nM	102.7
7.8 nM	102.4
0 nM	88.8

Table S2: Average experimental values and fits derived from varying the elongation, secondary nucleation, and primary nucleation rate constants, k_+, k_2, and k_n, respectively.

Inhibitor	k_+ (raw)	k_2 (raw)	k_n (raw)	k_+ (scaled)	k_2 (scaled)	k_n (scaled)
250 nM	1.4e+05	3.5e-04	1.5e-10	5.9e-02	5.2e-08	3.7e-07
125 nM	4.7e+05	1.9e+02	1.1e-06	2.0e-01	2.9e-02	2.7e-03
62.5 nM	9.4e+05	1.4e+03	1.9e-05	3.9e-01	2.1e-01	4.7e-02
31.3 nM	1.8e+06	4.3e+03	1.7e-04	7.6e-01	6.5e-01	4.3e-01
15.6 nM	1.8e+06	4.5e+03	1.8e-04	7.7e-01	6.8e-01	4.6e-01
7.8 nM	1.8e+06	4.3e+03	1.8e-04	7.6e-01	6.5e-01	4.6e-01
0 nM	2.4e+06	6.7e+03	4.0e-04	1.0e+00	1.0e+00	1.0e+00

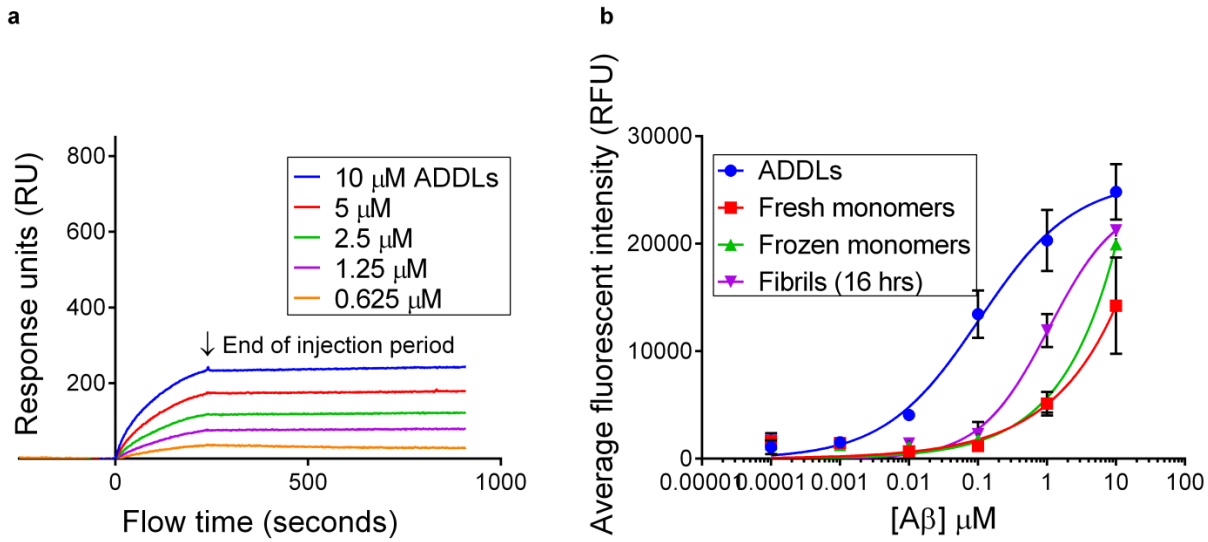

SUPPLEMENTARY FIGURE 1. Analysis of PrP binding to Aβ monomers, fibrils, and ADDLs. (a) ADDLs were subjected to SPR analysis as in Fig. 5 a, b **(b)** PrP binding of the indicated concentrations (in monomer-equivalents) of Aβ monomers (fresh and frozen), fibrils (polymerized for 16 hrs), and ADDLs was analyzed by DELFIA. Averages are for triplicate measurements.

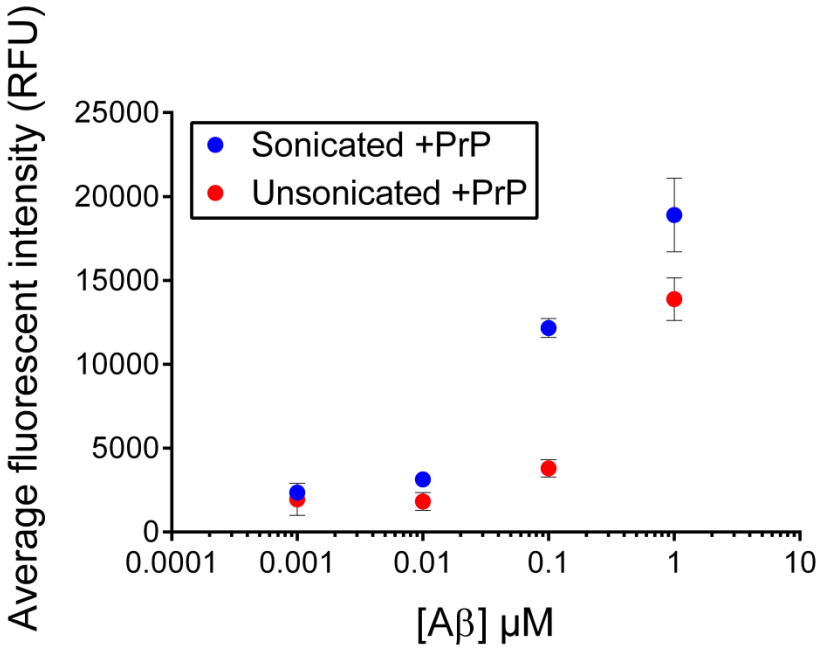

SUPPLEMENTARY FIGURE 2. Sonication of Aβ fibrils increases binding to PrP. Aβ fibrils polymerized for 16 hours were subjected to sonication for 10 minutes, and binding to PrP was compared to unsonicated fibrils at identical monomer-equivalent concentrations by DELFIA.

References

1. Cohen, S. I., Vendruscolo, M., Dobson, C. M., and Knowles, T. P. (2011) Nucleated polymerization with secondary pathways. III. Equilibrium behavior and oligomer populations. *Journal of Chemical Physics* **135**, 065107
2. Cohen, S. I., Vendruscolo, M., Dobson, C. M., and Knowles, T. P. (2011) Nucleated polymerization with secondary pathways. II. Determination of self-consistent solutions to growth processes described by non-linear master equations. *Journal of Chemical Physics* **135**, 065106
3. Cohen, S. I., Vendruscolo, M., Welland, M. E., Dobson, C. M., Terentjev, E. M., and Knowles, T. P. (2011) Nucleated polymerization with secondary pathways. I. Time evolution of the principal moments. *Journal of Chemical Physics* **135**, 065105
4. Cohen, S. I., Linse, S., Luheshi, L. M., Hellstrand, E., White, D. A., Rajah, L., Otzen, D. E., Vendruscolo, M., Dobson, C. M., and Knowles, T. P. (2013) Proliferation of amyloid-β42 aggregates occurs through a secondary nucleation mechanism. *Proc. Natl. Acad. Sci. USA* **110**, 9758-9763
5. Arosio, P., Michaels, T. C., Linse, S., Mansson, C., Emanuelsson, C., Presto, J., Johansson, J., Vendruscolo, M., Dobson, C. M., and Knowles, T. P. (2016) Kinetic analysis reveals the diversity of microscopic mechanisms through which molecular chaperones suppress amyloid formation. *Nat. Commun.* **7**, 10948
6. R Core Team. R: A language and environment for statistical computing (2015). Vienna, Austria: R Foundation for Statistical Computing. https://www.R-project.org/
7. Elzhov, T.V., Mullen, K.M., Spiess, A-N, and Bolker, B. (2015) Minpack.lm: R interface to the levenberg-marquardt nonlinear least-squares algorithm found in mINPACK, plus support for bounds. http://CRAN.R-project.org/package=minpack.lm
8. Warnes, G.R., Bolker, B., Gorjanc, G., Grothendieck, G., Korosec, A., Lumley, T., MacQueen, D., Magnusson, A., Rogers, J., *et al*. (2015) Gdata: Various R programming tools for data manipulation. http://CRAN.R-project.org/package=gdata
9. Wickham. H. Ggplot2: Elegant graphics for data analysis. (2009) Springer-Verlag New York; http://ggplot2.org

Cellular prion protein targets amyloid-β fibril ends via its C-terminal domain to prevent elongation

Erin Bove-Fenderson, Ryo Urano, John E. Straub and David A. Harris

J. Biol. Chem. 2017, 292:16858-16871.
doi: 10.1074/jbc.M117.789990 originally published online August 23, 2017